Journal of Bio- and Tribo-Corrosion (2020) 6:77
https://doi.org/10.1007/s40735-020-00369-4

Effect of Bio-Fluid on the Corrosion Properties of Tungsten Surface Alloyed Under Nitrogen on Austenitic Stainless Steel

M. Krishnakumar[1] · R. Saravanan[1] · Vijay Narayanan[1]

Received: 23 September 2019 / Revised: 17 April 2020 / Accepted: 7 May 2020 / Published online: 24 May 2020

Abstract
Stainless steel is mostly used in applications where resistance to corrosion is of prime importance. The surface-treated stainless steels are widely used in many applications. AISI304 stainless steel has a low surface hardness and a relatively high wear rate. AISI304 stainless steel bar and Tungsten (W) were chosen as the substrate and the alloying material, respectively. The W powder was pasted over the surface of the AISI304 stainless steel using a PVA binder. The surface modification process was carried out using the heat generated by a Gas Tungsten Arc (GTA). The corrosion behavior of substrate and surface alloyed. AISI304 stainless steel was studied using the TAFEL polarization test. The corrosion was studied in Hanks balance salt solution. The study revealed that pitting corrosion occurs on the surface of the specimens, but I_{corr} value increased by an order of magnitude two. The increase in corrosion current is attributed to the formation of the oxides, and carbides formed in the surface of the modified layer. This implies that surface alloying with W enhances the corrosion resistance of the AISI304 stainless steel. The investigation concludes that the surface alloying process with W using GTA is effective for modifying the surface properties of AISI304 stainless steel.

Keywords AISI304 stainless steel · Corrosion · Bio-fluid · Tungsten · Surface alloying

1 Introduction

Stainless steel (SS) is mainly used in places where high surface hardness and high wear rate has been key obstacles to extensive application. SS has been extensively utilized in aeronautical, aerospace, food processing, nuclear and biomedical and maritime industry because of its high corrosion resistance. In the atmosphere, chromium combines with oxygen to form a thin passive coating of chrome oxide on the surface of the SS. However, in case the SS is brought into contact with corrosive fluid, such as hydrogen sulfide, chlorine ion, and hot water containing oxygen, pitting corrosion or cracks due to corrosion are liable to occur in the surface of the SS. Typical products of SS such as surgical instruments, control rod cases in nuclear power plants, tools, and mold, gears, screws, valves, pump parts, bearings, filters, orthopedic parts are subjected to surface treatment processes to increase the surface properties without influencing the bulk properties [1, 2].

The 18–8 stainless steel has excellent resistance to corrosion by weak bases such as ammonium hydroxide and organic compounds like aniline, pyridine, and aliphatic amines. Type 304 SS can be used for such equipment as ammonia stills and certain types of amination reactions. The performance of stainless steels in solutions of strong bases may be illustrated with results of tests in sodium hydroxide solutions, the 18–8 steel usually shows a very slight attack in solutions up to 50% NaOH. In higher concentrations and temperatures corrosion rates are likely to be appreciable. Under conditions of stress, stress corrosion cracking of stainless steels may occur in hot sodium or potassium hydroxide solutions. Hot metal surfaces wetted by dilute solutions may be so affected due to the concentration of the caustic by evaporation [3]. To increase the corrosion resistance of SS implants a big effort has been developed to form a bioactive titanium oxide layer on the metal surface using several ways

✉ R. Saravanan
r_saravana@cb.amrita.edu

M. Krishnakumar
mahavin1996@gmail.com

Vijay Narayanan
vjn6051@gmail.com

[1] Department of Mechanical Engineering, Amrita School of Engineering, Amrita Vishwa Vidyapeetham, Coimbatore 641112, India

as chemical, electrochemical, thermal treatment, and anodization methods among others [4, 5]. Titanium offers advantages such as good mechanical properties as well as corrosion resistance under biological fluid conditions, although the material high cost is a holdup. Similar behavior of the Ti alloyed SS implant obtained by maintaining titanium in contact with bone and body tissue (aqueous solution) without diminishing its mechanical properties, at a lower cost [6]. It also indicates that the Ti sub-layer can enlarge the pseudo-diffusion layer and enhance the adhesion strength of TiN coatings. For the TiN/Ti double-layered coating, good corrosion resistance can be obtained with the measured ultimate shear stress higher than 10 GPa and the inter-diffusion zone thicker than 0.2 mm [7]. Ti ions were implanted into electroless nickel coating at 100 keV and 5×10^{16}–3×10^{17} ions/cm^2 using a metal plasma ion implantation apparatus. The corrosion resistance of Ti-implanted electroless nickel was improved by the formation of chemically inert titanium oxides and Ti–Ni alloys in the ion-implanted layer, which leads to the increase of polarization resistances in the EIS analysis [8].

The $Cr_{23}C_6$ precipitation was observed after the sensitization of AISI304 SS specimens in the neutral flame by using oxy-fuel and slowly cooled in the air. The microstructure of AISI304 SS shows the pitting corrosion resistance properties as the sensitization time increases. As the specimens were rapidly cooled due to quenching the $Cr_{23}C_6$ precipitate was dissolved and improved corrosion resistance [9]. Corrosion behavior of TiN coated SS was studied on the specimens with the controlled coating thickness. The electropolarization technique was used to evaluate the corrosion resistance of the coated samples under 5% NaCl and 1 N H_2SO_4 + 0.05 KSCN. The effect of coating thickness and the packing factor plays an effective role in the corrosion resistance of the coated samples [10]. Duplex TiN coatings were deposited on AISI 304 stainless steel with arc-ion plating. The corrosion performance of the duplex TiN coatings was evaluated in an acidic chloride solution by using electrochemical techniques such as potentiodynamic polarization and EIS analysis. The oxide film formed on the TiN coating is an important factor influencing the corrosion performance of the coated substrate [11]. Pressurized metallurgy remarkably enhanced nitrogen (N_2) content in martensitic stainless steel. Increasing N_2 content firstly decreased and then increased the content of precipitates. With increasing N_2 content, precipitates were converted from $M_{23}C_6$ to M_2N high nitrogen martensitic stainless steels exhibiting excellent corrosion resistance. Excess nitrogen deteriorated corrosion resistance of martensitic stainless steel [12].

The surface of AISI304 SS was melted in argon (Ar) and nitrogen (N_2) atmosphere using different laser beam scan rate and gas flow. The electrochemical studies reveal the reduction in the formation of pits in the surface melted under the N_2 gas environment [13]. Laser surface alloying (LSA) under optimum conditions significantly improves the pitting corrosion resistance in terms of critical potential for pit formation and pit growth. Besides, the erosion resistance in 20 wt% and in 3.56 wt% NaCl solution registers a marked improvement. Thus, it is concluded that the LSA of 304 SS with Mo is an appropriate technique to enhance the resistance to pitting and erosion in stainless steel [14]. To improve the surface properties ofAISI304 SS, laser surface alloying was performed on the surface of AISI304 SS coated WC, Ni, Co, and Cr. The surface properties of the substrate increased drastically [2, 15, 16]. The surface of AISI304 SS was alloyed with W + Ti under Ar and N_2 using GTA to improve the mechanical and corrosion properties. The surface of AISI304 SS was refined by Ti, and W particulates were dispersed on the alloyed surface thus increasing the mechanical properties and corrosion resistance of the alloyed layer [17, 18]. A vacuum arc remelting furnace was used to remelt SUS 304 stainless steel with various added Cu contents. The corrosion test indicates that the pitting potential declines as the Cu content in SUS 304 steel increases. The results of the antibacterial test reveal that adding a proper amount of Cu gives SUS 304 stainless steel an excellent antibacterial property [19].

Previous studies report the occurrence of pitting corrosion of various alloying elements alloyed using various alloying techniques in saline medium evaluated using TAFEL polarization testing. The objective of this study is to evaluate the corrosion nature of the pure W powder alloyed on the surface of AISI304 SS under the Ar and N_2 shielding environment in a simulated bio-fluid extracted from bone and body tissues which is Hanks Balanced Salt Solution without phenol red.

2 Experimental Procedure

A standard dimension ($150\times30\times30$ mm^3) of AISI304 SS was procured and cleaned with acetone to remove dust, oxides, and other containments on the top surface and then taken to arc spectroscopic analysis. The arc spectroscopic analysis reveals the chemical composition of the substrate. Table 1 shows the chemical composition of the AISI 304 stainless steel. The substrate was pasted with a mixture of W powder on the surface of the substrate using poly-vinyl alcohol (PVA) as a binder. The pasted substrate was kept in resistive type heat treatment furnace at 90 °C for 30 min to remove moisture on the pasted surface. The GTA heat source shielded with Ar and mixed constant flow of N_2 was used to modify the surface of the substrate and the pasted surface. The samples were named as A, N, W, and WN, respectively. Samples A and N represent the only surface-refined layer under Ar and N_2 shielding environment, respectively. Similarly, samples named W

Table 1 Chemical composition of AISI 304 SS

Element	Cr	Ni	W	N	Ti	C	Fe
Wt%	18.25	8.18	0.047	0.031	0.004	0.003	Balance

Table 2 GTA process parameter

Sample ID	Process parameters					
	Current	Travel speed	Electrode	Gas flow	Standoff distance	Electrode diameter
A, NW, WN	200 A	2 mm/s	2% Thoriated tungsten	12 L/min	3 mm	3 mm

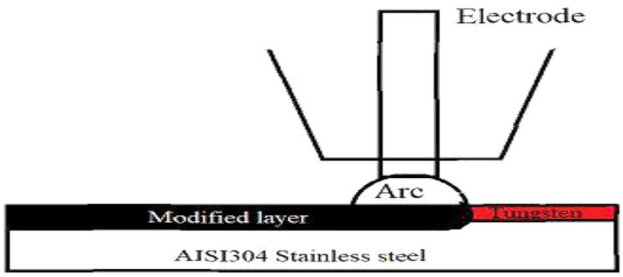

Fig. 1 Experimental setup of surface modification process

and WN represent the surface-modified in the W pasted layer under Ar and N_2 shielding environment, respectively. Table 2 shows the process parameters used for the surface modification process (SMP). Figure 1 shows the experimental setup of SMP. After the surface modification, the modified samples were sliced using electric discharge machine wire cutting and the sliced samples were finely polished for electropolarization testing. The substrate and the surface-modified specimens were sliced to a dimension of 15 mm × 5 mm × 4 mm for corrosion testing. These specimens were mechanically polished using different grades of emery paper followed by diamond polisher to achieve a mirror finish and cleaned with acetone to remove the impurities. Potentiodynamic polarization tests were conducted in Hanks Balance Salt Solution (HBSS) which is a synthesized bio-fluid. Table 3 shows the composition of the HBSS. The potentiodynamic polarization curve of each specimen was measured between − 0.5 and 0.5 mV/s of open circuit potential (OCP) at a potential scan rate of 0.1 mV/s was measured. Saturated calomel electrode (SCE) was used as the reference electrode, the platinum wire is used as a counter electrode, and the surface-modified specimens were used as a working electrode.

3 Results and Discussion

3.1 Surface Alloying Process

The temperature at the outer edge rapidly rises well above the solidus and the W dissolves into solution. The composition shifts toward the W-rich side of the miscibility gap in the intermetallic phases. The formation of intermetallic phases and the dispersion of W particles near the grain boundaries is due to the rapid cooling in the alloyed layer. The melting efficiency of GTA welding increases with the increase in current intensity. Fine-grained material is harder and stronger than coarse-grained. The Hall–Petch equation shows the yield strength which varies with grain size. Equation 1 shows the Hall–Petch equation

$$\sigma_y = \sigma_0 + k_y d \tag{1}$$

where σ_y is the yield strength, σ_0 and k_y are the constant for particular materials, and d is the average grain diameter. The grain size may be regulated by the rate of solidification from the liquid phase. The grain size reduction improves the strength and toughness of AISI304 SS. The alloys are stronger than pure metals because impurity atoms that go into solid solution ordinarily impose lattice strains on the strains on the surrounding host atoms. Lattice strain interactions between dislocation and the impurities atoms results and consequently restricted the dislocation movement [20]. The W particles in the alloyed surface are dispersed in the interstitial position of the lattice strain, thus restricting the dislocation movement and formed the smaller grain improving the surface hardness of the AISI304 SS from 277 to 1489 HV for W and 2010 HV for WN specimens, respectively. Figure 2 shows the surface hardness of the alloyed layer along the depth direction. Figure 3 shows the SEM micrograph of the surface alloyed layer reveling the dispersion of

Table 3 Chemical compositions of HBSS

Element	Nacl	KCl	$CaCl_2$	$MgSO_4$	$MgCl_2 - 6H_2O$	$Na_2HPO_4 - H_2O$	KH_2PO_4	$NaHCO_3$	$C_6H_{12}O_6$
Wt%	0.14	0.05	0.13	0.14	0.05	0.003	0.04	0.04	0.03

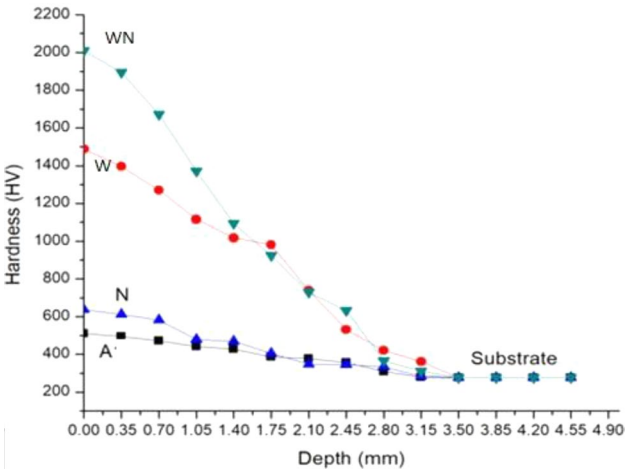

Fig. 2 Hardness along the depth direction

W in the alloyed layer and the refinement of grain structure. From Fig. 3a, b it is seen that the equiaxed grain structure has been transformed to refined dendrites structures. The reason for obtaining the dendritic structure is the large difference between the melting points of iron and other phases formed by the dissolution of N_2 gas in the modified layer. From Fig. 3c, d, the W particles have dissolved and dispersed in the modified layer uniformly throughout the dendritic structure as there is an increase in temperature at the outer edge of the W particle.

3.2 TAFEL Polarization

The electrochemical impedance spectrum (EIS) of the substrate and the modified surface layer is shown in Fig. 4. From Fig. 4 it is seen that the alloying under the N_2 atmosphere has a higher impedance in the EIS spectrum. The TAFEL polarization corrosion test was conducted to evaluate the anodic and cathodic behavior of the substrate and the alloyed layer. The TAFEL polarization curves of the substrate and the alloyed layer in HBSS is shown in Fig. 5. From the

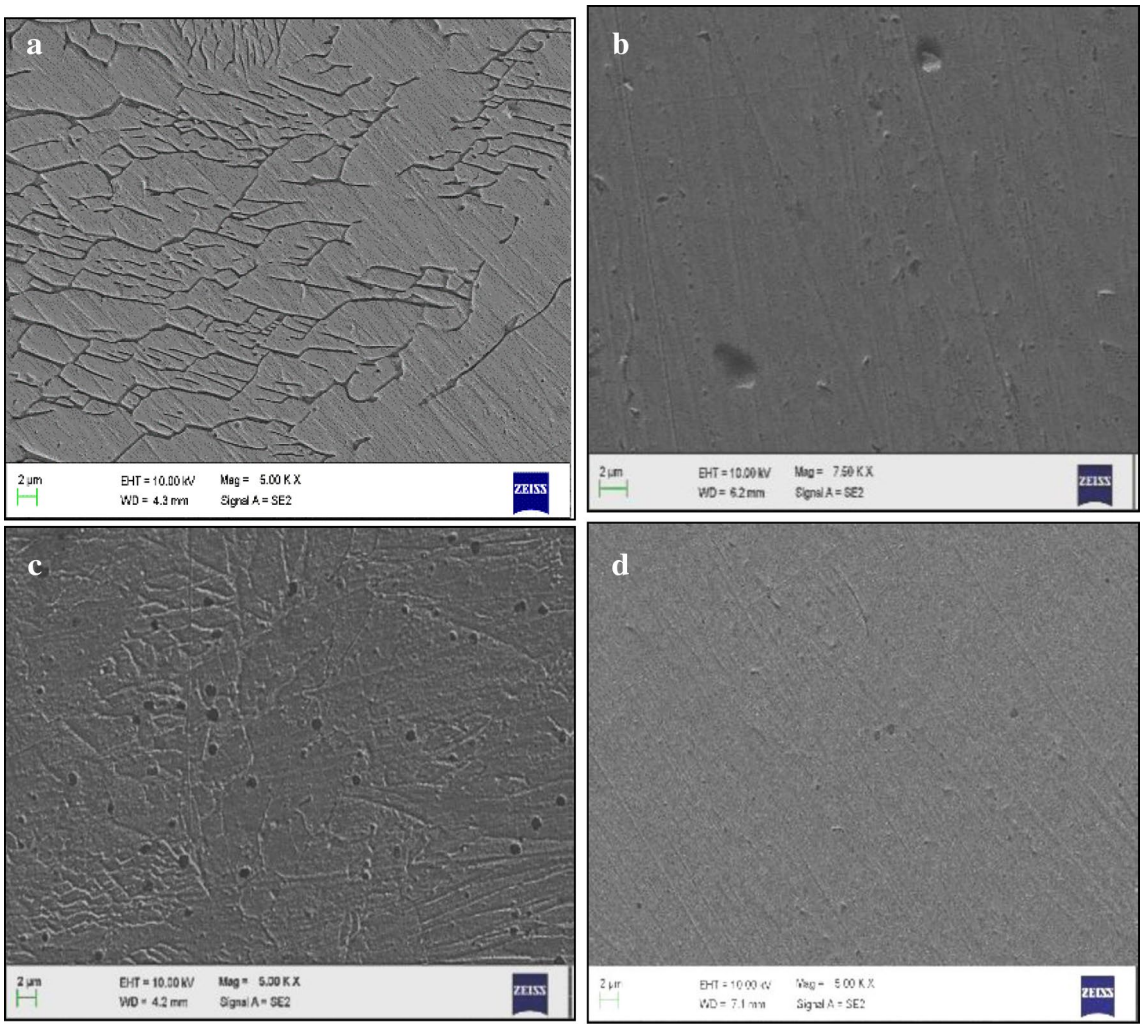

Fig. 3 SEM image of the modified layer **a**, **b** Sample A and N **c**, **d** Sample W and WN

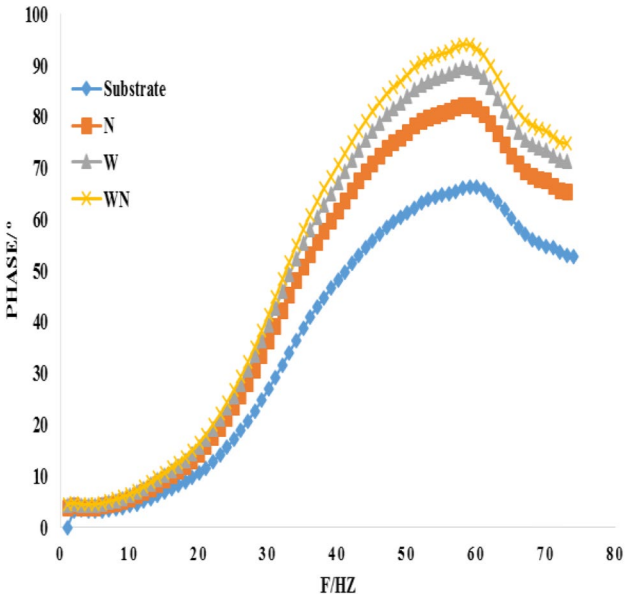

Fig. 4 Electrochemical impedance spectrum

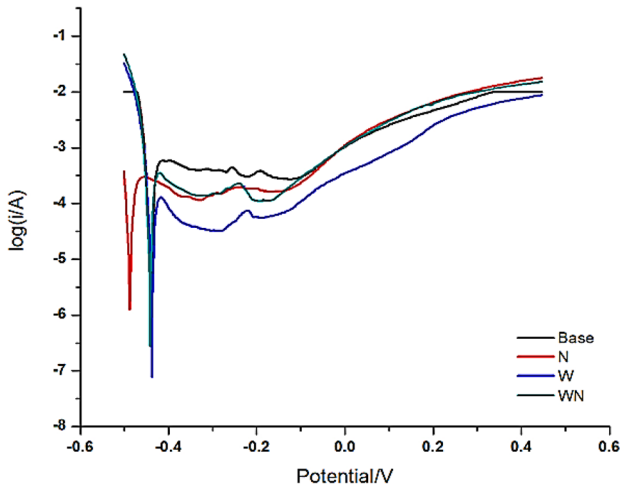

Fig. 5 TAFEL polarization curve

TAFEL polarization curve, the potential at which the rate of cathodic reaction equals the rate of anodic dissolution is known as corrosion potential (E_{corr}) [7, 8]. The corrosion potential (E_{corr}), the equilibrium corrosion current density (i_{Corr}), and the corrosion rate of the substrate and the SAL specimens were determined using Tafel extrapolation method and are summarized in Table 4. Moreover, increased surface hardness in W and WN specimens, especially the formation of intermediate phases on the surface, may also significantly improve the corrosion resistance of the modified layer. The evolution of H_2 gas from the electrolyte is the primary reaction in the cathodic reaction stage, as given by Eq. 2 [21, 22]. The dissolution of iron is the primary reaction in the anodic dissolution stage, as given by Eq. 3 [23, 24].

$$2H_2O + 2e^- \rightarrow H_2 \uparrow + 2OH \quad (2)$$

$$Fe \rightarrow Fe^{2+} + 2e \quad (3)$$

In the base material, the current increased with an increase in potential beyond the E_{corr}, which indicates a high anodic dissolution rate of iron. In the SAL, increase in current from 7.697×10^{-4} to 1.023×10^{-4}A was observed with an increase in potential up to − 0.412 mV and − 0.380 mV, similarly in the SML with N2 a small increase in current was observed with an increase in potential up to − 0.498 mV and − 0.397 mV. The presence of a protective film of corrosion products is attributed to this passivation tendency in the composite specimen. Further, the increase in potential beyond caused the breakdown of the film of corrosion products and increased the anodic dissolution of iron. Hence, an increase in the magnitude of current was observed.

In the potentiodynamic polarization plot, the region between $E_{corr} \pm 20$ mV is the TAFEL region. The tangents were drawn for the cathodic polarization branch and anodic polarization branch of the potentiodynamic polarization curve to intersect in the TAFEL region. The intersection point of the tangents corresponds to the corrosion current (i_{corr}) [25–27]. The i_{corr} was used to calculate the corrosion rate of the specimens using Eq. 4 [28, 29].

$$\text{Corrosion Rate} = \frac{k \times i_{corr} \times E'}{A \times \rho} \quad (4)$$

where k is a constant for representing the corrosion rate in terms of mm/year, i_{corr} is corrosion current in Ampere, E'

Table 4 TAFEL polarization curve result

Sample ID	Potentiodynamic scan				
	E_{corr} (mV)	I_{Corr} (A) ($\times 10^{-4}$)	Corroded area (E') (cm)	Equivalent weight (A)(g)	Corrosion rate (mmpy)
Base	− 0.412	7.697	0.37	0.09	0.628
N	− 0.498	6.152	0.26	0.09	0.502
W	− 0.380	1.023	0.35	0.09	0.167
WN	− 0.397	4.152	0.33	0.09	0.339

is the equivalent weight of the corroding specimen, given by the ratio of molecular weight to the number of electrons involved in the electrochemical reaction, A is exposed area in cm^2, and ρ is the material density of specimen in g cm^{-3}. It is observed from the results that the corrosion potential of the alloyed layer shifted cathodically compared to the substrate. This indicates that the modified specimens have better corrosion resistance in the HBSS in which the measurement was taken. The corrosion resistance (R_p) is a quantitative parameter that indicates the degree of protection offered by the passive layer formed over the SAL [30–32]. R_p is defined as the slope of the polarization curve at the corrosion potential, whose mathematical representation is given by Eq. 5. Stern–Geary Eq. 6 describes the relationship between the polarization resistance and corrosion current [33].

$$R_p = \frac{\Delta E}{\Delta I} \tag{5}$$

$$R_p = \frac{\beta_a \times \beta_c}{2.3 \times (\beta_a + \beta_c)} + \frac{1}{i_{corr}} \tag{6}$$

The R_p of the base material was 0.53 kΩ and that of the N, W, and WN SAL was 0.81 kΩ, 3.714 kΩ, and 0.95 kΩ, respectively. Comparing the R_p values, the polarization resistance of N, W, and WN SAL is ~ 1.5, ~ 7 and ~ 1.7 times higher than that of the base material in HBSS, respectively. This is a clear indication of higher corrosion resistance of the composite. The corrosion current density of the N, W, and WN modified specimen was about 20%, 86%, and 46% lower than that of the substrate, indicating a substantial improvement in the corrosion resistance. TAFEL curves of both the substrate and the modified specimen's show the initial anodic passivation, followed by strong localized corrosion, and further passivation. The modified surface shows passive corrosion at much higher corrosion currents, though for a slightly lower potential window. From Fig. 6 the base and the alloy exhibit a similar type of cathodic reaction. This indicates the triviality of the W – particles on the cathodic reaction. The W – particles are influential on the anodic dissolution of the alloyed layer. Eventually, all the SEM micrograph results portray a stable protective film developed on the surface of the modified layer. Hence, GTA treatment and W addition have a positive influence on the corrosion behavior of the AISI304 stainless steel. It is found from the TAFEL analysis that the corrosion rate of N modified (0.502 mmpy), W-modified (0.167 mmpy), and W-modified under nitrogen (0.339 mmpy) layers is much lower than that of the substrate (0.628 mmpy). Figure 5a, b shows SEM images of pitting corrosion after the corrosion test on the substrate and N-modified layer. Figure 6c shows the protective coating over the W specimen. It was noticed that the pitting corrosion is narrow and smaller for W specimen as compared to the substrate surface as shown

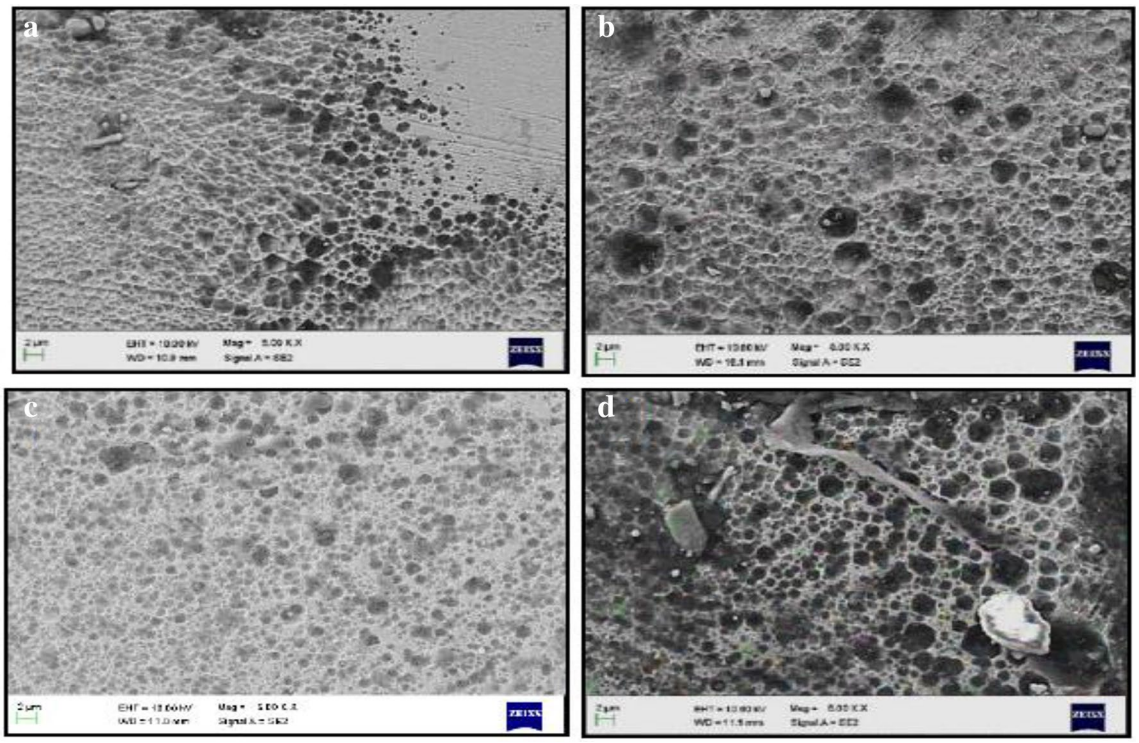

Fig. 6 Surface morphology of the specimens after potentiodynamic polarization analysis (**a**) Substrate, (**b**–**d**) sample N, W and WN

in Fig. 6d. During electrochemical analysis, the modified layer which acts as a passive layer attributes to the reduction in the pitting corrosion. The HBSS is rich in hydrogen phosphate, phosphate, and chloride ions. The small radius of chloride ions favors preferential adsorption of chloride ions on the surface of iron hydroxide. This subsequently favors the formation of iron chloride by replacement of hydroxide ions in iron hydroxide, as described by Eq. 7. The solubility of iron chloride is higher than that of iron hydroxide, which increases the sites for corrosion and promotes more dissolution of iron. Hence, the corrosion rate was quite higher during the initial period of immersion

$$Fe^{2+} + 2Cl^{-} \rightarrow FeCl_2 \tag{7}$$

$$3Ca^{2+}\ 2PO_4^{3-} \rightarrow Ca_3(PO_4)_2 \tag{8}$$

$$3Fe^{2+} + 2PO_4^{3-} \rightarrow Fe_3(PO_4)_2 \tag{9}$$

The elemental composition of the corroded region was analyzed using EDS. The EDS spectrum is shown in Fig. 7. It is observed that the analytical region consisted of iron, chromium, nickel, tungsten, titanium, nitrogen, sodium, calcium, phosphorus, potassium, chlorine, magnesium, sulfur, and oxygen elements. The elemental map of the corroded region with corrosion products formed in A, N, W, and WN is shown in Figs. 8, 9, 10, and 11, respectively. Figure 8 confirms that oxygen and carbon have entirely covered the surface of the corroded specimen, which indicates the formation of corrosion products or corrosion layers rich in calcium and phosphorous. Similarly in Figs. 9, 10, and 11 confirms that carbon, oxygen has entirely covered the surface of the corroded specimens. The major element next to iron, chromium, and nickel was found to be carbon, which is indicative of the corrosion product or corrosion layer rich in carbon. The elements sodium, chlorine, and calcium were also found to be deposited on the surface. Figure 12 shows the XRD graph of the corroded specimens. The major and minor peaks are between 43° to 44° and 70° to 80°, which is an indication of the presence of corrosion products. The XRD spectrum proves the corrosion formed are carbides and oxides. The formation of such an adherent layer of corrosion products decreased the corrosion rate of the specimens in the later stages of TAFEL polarization. A fine dispersion of W particulates and the formation of corrosion products decreases the corrosion rate of the SAL. The corrosion products formed were found using the XRD spectrum. The formed corrosion products are found to be NiC, NiO, $Cr_{23}C_6$, and Fe_3C on the substrate, and NiO, NiC, Cr_3O, W_3O, and Fe_2O_4 on W and WN specimens. The formed corrosion products were

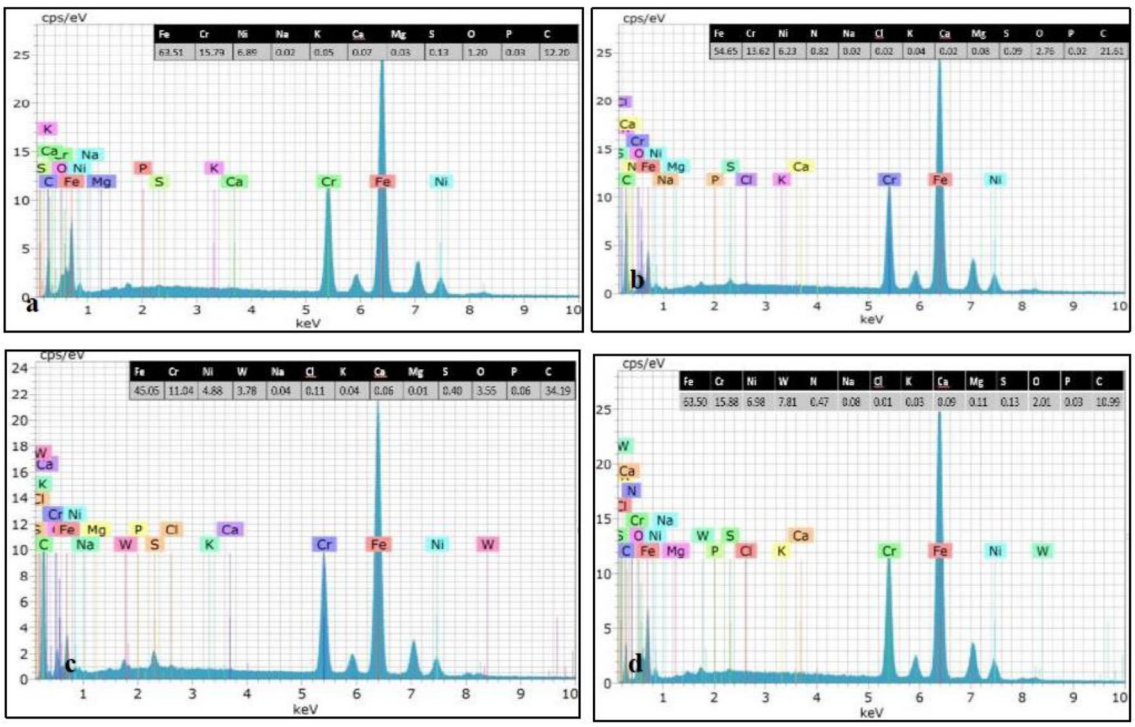

Fig. 7 EDAX spectrum on the pitting corrosion of the substrate (**a**) N, W, WN specimens (**b**–**d**)

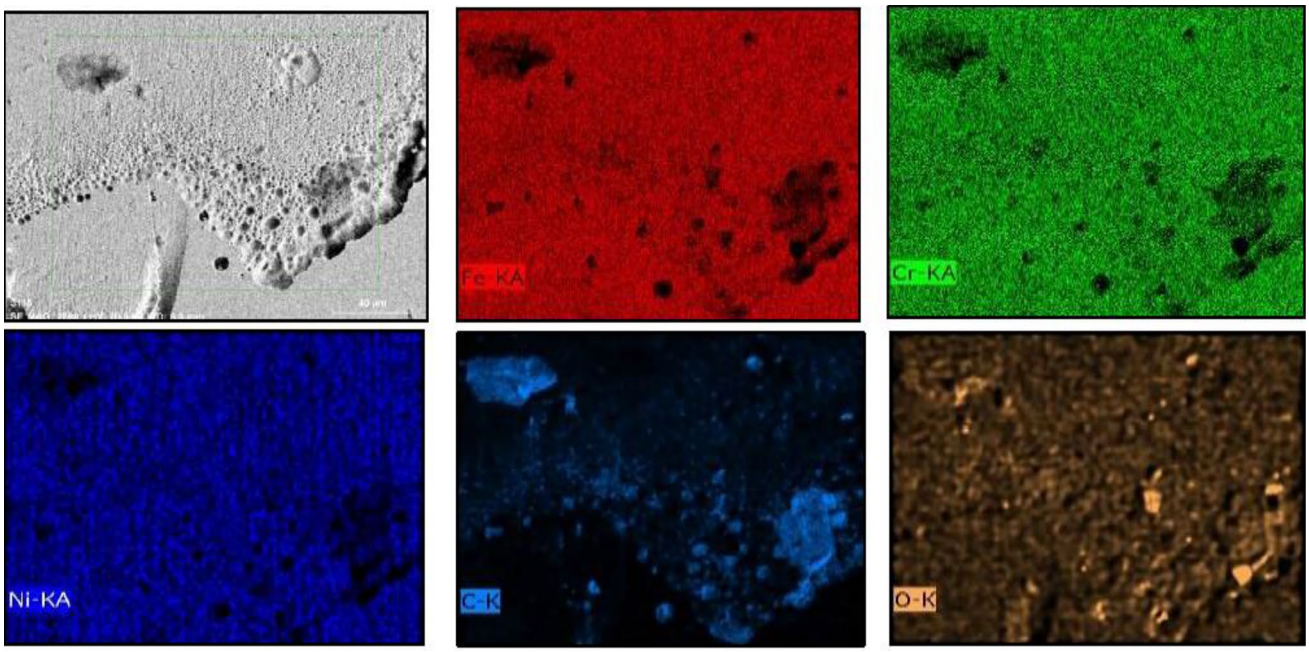

Fig. 8 Elemental mapping on the corroded surface of the substrate

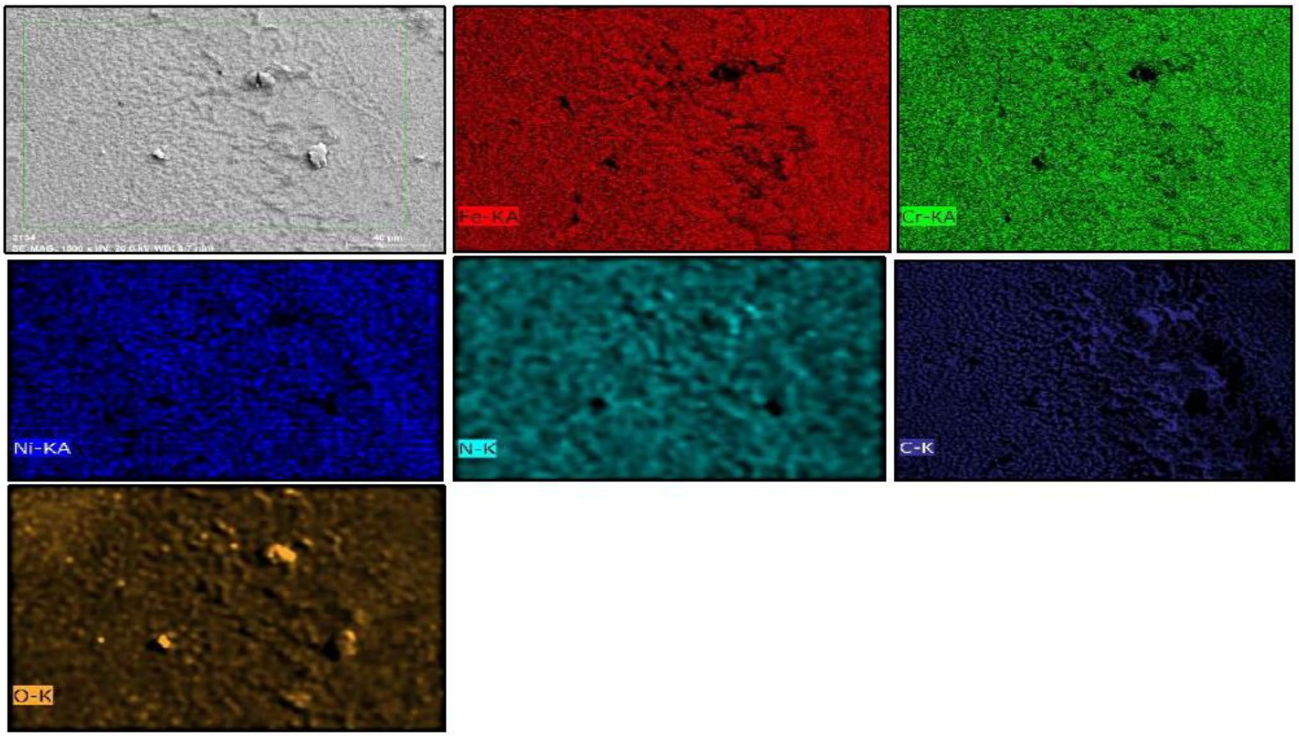

Fig. 9 Elemental mapping on the corroded surface of the N specimen

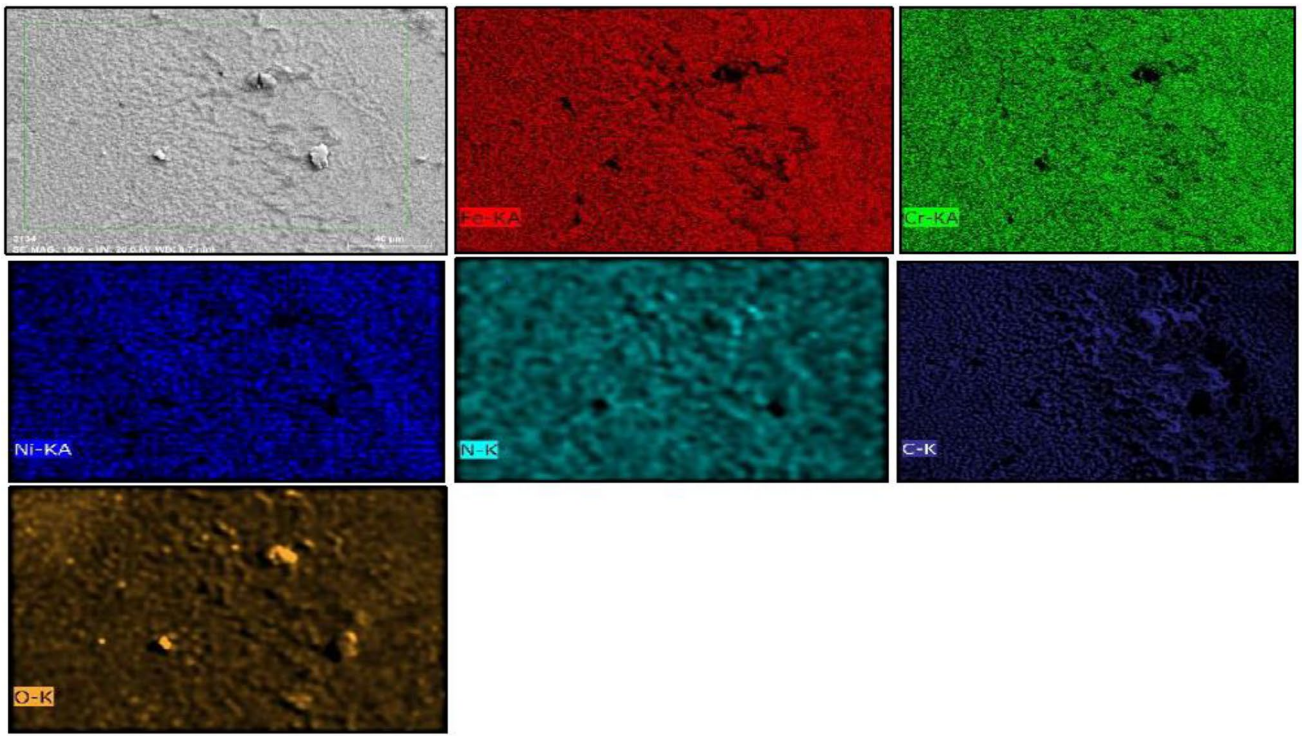

Fig. 10 Elemental mapping on the corroded surface of the W specimen

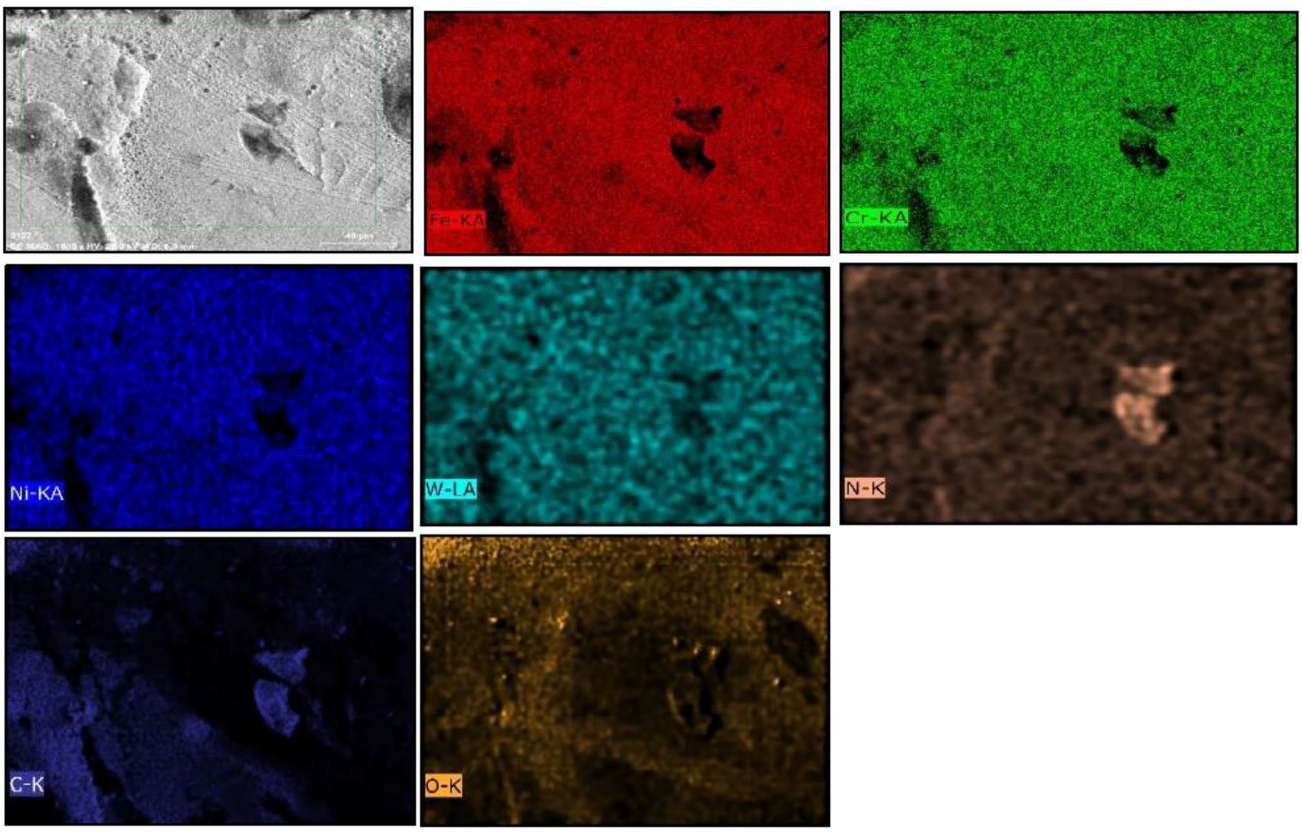

Fig. 11 Elemental mapping on the corroded surface of the WN specimen

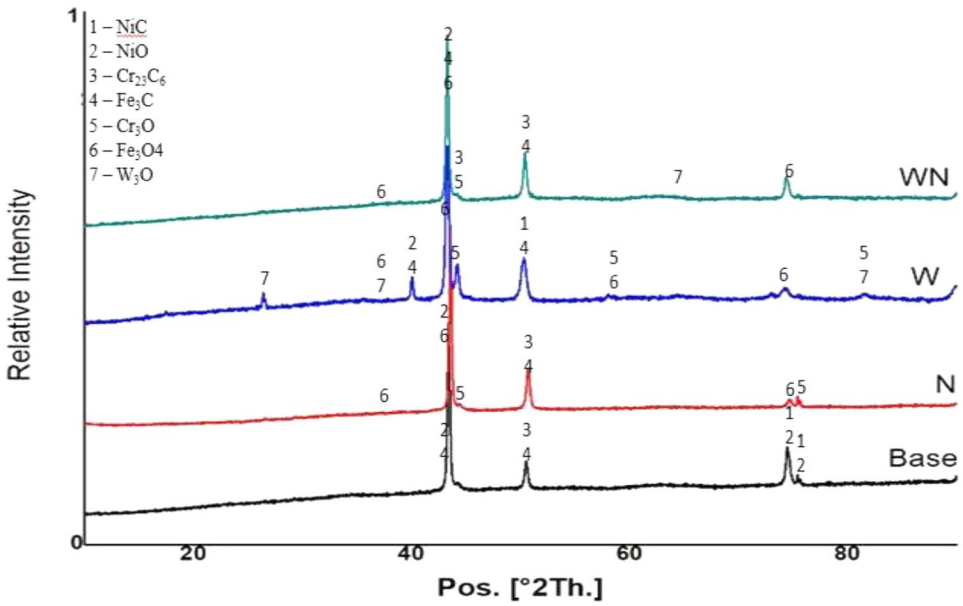

Fig. 12 XRD spectrum of the corroded surface

confirmed with the 03-0920, 83-0878, 65-4828, 89-7069, and 79-2159 ICDD – JCPDS data of NiO, NiC, Cr_3O, W_3O, and Fe_2O_4 intermetallic phases.

4 Conclusions

The corrosion behavior of the 304 SS substrate and the modified layer was studied using Potentiodynamic polarization analysis in HBSS (pH ~ 7.2). The result observed is summarized as follows.

- The surface alloying process of AISI304 stainless steel with Tungsten increases the corrosion resistance of the AISI304 stainless steel.
- The corrosion potential value is found to increase from – 0.412 V for the substrate to – 0.380 V, – 0.397 V for the tungsten surface alloyed layer under argon and nitrogen environment, respectively.
- The corrosion current value is found to increase from 7.697×10^{-4} A for the substrate to 1.023×10^{-4} A for the W surface alloyed layer which delays corrosion.
- The corrosion resistance is found to increase from 0.628 mmpy for the substrate to 0.167 mmpy for the tungsten surface alloyed layer
- The corrosion mechanism occurring in the AISI304 stainless steel substrate and W surface alloyed layer is found to be galvanic pitting corrosion.
- The formation of oxides, chlorides, nitrides, and carbides improves the corrosion resistance of the W surface alloyed layer under the argon and nitrogen atmosphere.
- The surface alloying of AISI304 stainless steel with W using GTA under argon and nitrogen atmosphere can be identified as a worthy method to improve the corrosion resistance of the AISI304 stainless steel.

Acknowledgements The author would like to express heart-full gratitude to Dr. R. Sellamuthu Ph.D., Professor, Department of Mechanical Engineering, Amrita School of Engineering, deserves special thanks for the encouragement and advice throughout the work, and sincere gratitude for his constant support. The author would like to thank all the faculties, lab assistant and office staff of the Department of Mechanical Engineering of our School of Engineering for their help and support to carry out this work successfully.

References

1. Narayanan V, Saravanan R, Sellamuthu R (2016) An investigation on the hardness and wear rate of surface alloyed AISI304 stainless steel with Ti using GTA as heat source. Indian J Sci Technol 9:16
2. Krishnakumar M, Saravanan R, Sellamuthu R, Vijaynarayan (2018) Microstructure, hardness and wear rate of heat treated titanium surface alloyed AISI 304 stainless steel. Mater Today Proc 5:7571–7576
3. Jonasova L, Muller FA, Helebrant A, Strnad J, Greil P (2004) Hydroxyapatite formation on alkali-treated titanium with different content of Na+ in the surface layer. Biomaterial 25:1187
4. Brenemark PI, Prosthet J (1986) Osseointegration in skeletal reconstruction and rehabilitation: a review. Dentistry 50:399
5. Barragán F, Guardián R, Menchaca C, Rosales I, Uruchurtu J (2010) Electrochemical corrosion of hot pressing titanium

coated steels for biomaterial applications. Int J Electrochem Sci 5:1799–1809
6. Chen JY, Yu GP, Huang JH (2000) Corrosion beaviour and adhersion of ion-plated TiN film on AISI 304 Stainless steel. Mater Chem Phys 65:310–315
7. Chang YY, Wang DY (2005) Corrosion behavior of electroless nickel-coated AISI 304 stainless steel enhanced by titanium ion implantation. Surf Coat Technol 200:2187–2191
8. Warikh M, Rashid A, Miron G, Zulkifli MR, Asyadi Azam M (2012) Formation of $Cr_{23}C_6$ during the sensitization of AISI 304 stainless steel and its effect to pitting corrosion. Int J Electrochem Sci 7:9465–9477
9. Chou WJ, Ping G, Huang JH (2001) Corrosion behavior of TiN-coated 304 stainless steel. Corros Sci 43:2023–2035
10. Rudenja S, Leygraf C, Pan J, Kulu P, Talimets E, Mikli V (1999) Duplex TiN cotings deposited by arc palting for increased corrosion resistance of stainless steel substrate. Surf Coat Technol 114:126–136
11. Feng H, Jiang Z, Li H, Lu P, Zhang S, Zhu H, Zhang B, Zhang T, Xu D, Chen Z (2018) Investigation of microbiologically influenced corrosion of the high nitrogen nickel-free stainless steel by *Pseudomonas aeruginosa*. Corros Sci. https://doi.org/10.1016/j.corsci.2018.09.002
12. Conde AA, Garica I, de Damborenea JJ (2001) Pitting corrosion of 304 stainless steel after laser surface melting in argon and nitrogen atmospheres. Corros Sci 43(5):828–871
13. Majumdar JD, Manna I (1999) Laser surface alloying of AISI 304-stainless steel with molybdenum for improvement in pitting and erosion–corrosion resistance. Mater Sci Eng A 267:50–59
14. Xiong Y, Smugeresky JE, Schoenung JM (2009) The influence of working distance on laser deposited WC–Co. Mater Process Technol 209:4935–4941
15. Anandan S, Pityana S, Majumdar JD (2012) Structure–property-correlation in laser surface alloyed AISI 304 stainless steel with WC + Ni + NiCr. Mater Sci Eng A 536:159–169
16. Chakraborty A, Pityana S, Majumdar JD (2017) Laser surface alloying of AISI 304 stainless steel with WC+Co+NiCr for improving wear resistance. Proc Manuf 7:8–14
17. Krishnakumar M, Saravanan R (2019) Impact of tungsten on microstructure, hardness and wear rate of AISI 304 stainless steel surface alloyed under nitrogen environment. Mater Res Express 6:086571
18. Fan C, Li H, Kecskes LJ, Tao K, Choo H, Liaw PK, Liu CT (2006) Mechanical behavior of bulk amorphous alloys reinforced by ductile particles at cryogenic temperatures. Phys Rev Lett 96(14):145506
19. Fontana MG (1986) Corrosion engineering. McGraw-Hill, New York
20. Callister WD (2012) Materials science, and engineering. Wiley, Amsterdam, pp 361–362
21. Drogowska M, Meanard H, Brossard L (1997) Pitting of AISI 304 stainless steel in bicarbonate and chloride solutions. J Appl Electrochem 27:169–177
22. Ramalingam VV, Ramasamy P (2017) Modelling corrosion behavior of friction stir processed aluminium alloy 5083 using polynomial: radial basis function. Trans Indian Inst Met 70:2575–2589
23. Vaira Vignesh R, Padmanaban R, Datta M (2018) Influence of FSP on the microstructure, microhardness, intergranular corrosion susceptibility and wear resistance of AA5083 alloy. Tribol-Mater Surf Interfaces 12:157–169
24. Song GL, Atrens A (1999) Understanding magnesium corrosion—a framework for improved alloy performance. Adv Eng Mater 1:11–33
25. Zeng RC, Wang L, Zhang DF, Cui HZ, Han EH (2014) In vitro corrosion of Mg-6Zn-1Mn-4Sn-1.5Nd/0.5Y alloys. Front Mater Sci 8:230–243
26. Ghali E, Dietzel W, Kainer K-U (2004) General and localized corrosion of magnesium alloys: a critical review. J Mater Eng Perform 13:7–23
27. Pourbaix M (2012) Lectures on electrochemical corrosion. Springer Science & Business Media, Berlin
28. Stansbury EE, Buchanan RA (2000) Fundamentals of electrochemical corrosion. ASM International, Ohio
29. Fontana MG (2001) Corrosion engineering. McGraw Hill Education, New York
30. Fontana MG (2005) Corrosion engineering. Tata McGraw-Hill Education, New York
31. Marcus P (2011) Corrosion mechanisms in theory and practice. CRC Press, Boca Raton, FL
32. Kelly RG, Scully JR, Shoesmith D, Buchheit RG (2002) Electrochemical techniques in corrosion science and engineering. CRC Press, Boca Raton, FL
33. Schulte F (1976) A theory of thin metal films: electron density, potentials and work function. Surf Sci 55:427–444